Micro-displacement Sensor based on Hollow Core Fiber Interferometers

A. Sanchez-Gonzalez[1,2], A. Rodriguez-Rodriguez[1,2], R. Dauliat[3], R. Jamier[3], P. Roy[3], R. A. Perez-Herrera[1,2] and M. Lopez-Amo[1,2]

[1]Department of Electrical, Electronic and Communication Engineering, Public University of Navarra, 31006 Pamplona, Spain.
[2]Institute of Smart Cities (ISC), Public University of Navarra, 31006 Pamplona, Spain.
[3]XLIM UMR CNRS 7252, University of Limoges, F-87000 Limoges, France
Author e-mail address: arturo.sanchez@unavarra.es

Abstract: An interferometric sensor based on hollow core fibers for the measurement of micro-displacement has been designed. Its characterization has resulted in a linear response, suggesting its application in pressure sensors. © 2022 The Author(s)

1. Introduction

Hollow core fibers (HCFs), characterized by an annular cross section of variable thickness and material, have historically been employed for two purposes. On the one hand, they are used in laser power delivery [1]. On the other hand, they are commonly used as optical fiber sensors. Among the latter, the advances made in temperature, strain, and gas detection sensors are particularly noteworthy. Although there are some examples in which they are also implemented as pressure sensors [2], all of them measure only homogeneously distributed pressures over the whole inner or outer surface of the fiber, and not on a particular direction. Consequently, we propose the use of these HCFs as a new type of interferometric sensor to evaluate transverse micro-displacement, whose principle of operation can be extended to monitoring point pressure.

2. Sensor Design

2.1. Dimensions

The sensor consisted of a 3 mm long section of HCF, spliced between two sections of single-mode fiber (SMF). This length, hence that of the sensor itself, was imposed by the dimensions of the experimental setup, as it will be seen later. Regarding the HCF cross-section, the outer diameter was set to 125 μm, matching the cladding diameter of the SMF and thus simplifying the subsequent splicing procedure. With respect to its inner diameter (ID), it should be chosen fairly large because, by widely exceeding the mode field diameter of the SMF employed, the impact of core collapse that might arise in the splices involved is minimized [3]. Nevertheless, the thickness of the cladding must be large enough to allow a wide range of mechanical deformation without rupture. Under both considerations, HCFs with different IDs ranging from 50 to 75 μm were tested. Finally, the 55 μm ID fiber offered the best trade-off between sensitivity and measuring range in the manufactured sensors. Therefore, the presented development focuses on this HCF.

2.2. Manufacturing

Firstly, regarding the two special HCF cuts involved in the manufacturing of the sensor, these were performed by an automated cleaver station. In it, two motorized clamps with 1 μm movement resolution were responsible for positioning the desired cleaving point of the fiber in the center of an 18 cm long rail, in which an electric cleaver awaited. These clamps integrate a load cell so that the fiber tensioning could be adjusted up to 1000 grams with a resolution of 1 gram. Once the cleaving spot was properly positioned and the fiber was strained, the electric cleaver was activated and its vibrating blade descended over the fiber until severed. The whole procedure was handled by software and aided by an optical microscope for the initial positioning of the desired cleaving spot on the center of the rail. The fiber-by-fiber fine tuning of vibration frequency, vibration amplitude, and blade speed parameters, as well as the strain exerted on the fiber, resulted in straight and homogeneous cleaves regardless of the HCF under consideration. Moreover, the movement resolution of the motorized clamps set the uncertainty in the length of the HCF section of the sensor down to 1 μm, which was under the interrogation wavelength. Taking into account that the manufactured sensor presented a HCF section length of 3 mm due to the experimental setup limitations, this meant a maximum error of 0.03 %.

Secondly, with regard to the fusions involved, a specialty fiber fusion splicer (Fujikura FSM-100P) was employed. Hence, by properly adjusting the parameters of electrode location, discharge intensity, fuse time, and gap between

fiber ends, it was possible to guarantee fusions capable of withstanding the strains applied by the automated cleaver station, but without causing significant core collapse in any of the cases. A picture of both splices of the resulting sensing structure can be observed in Fig. 1 (c).

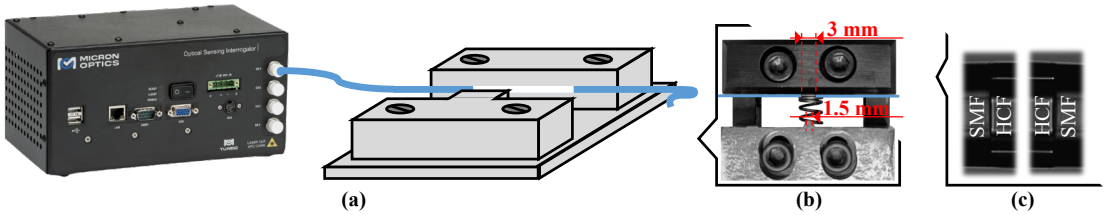

Fig 1. Schematic diagram of the experimental setup (a), detailed view of the mechanical actuator (b), and a picture of the sensor splices (c).

3. Experimental Setup

The setup employed in the study is shown in Fig. 1 (a). The operating principle of the sensor is based on the optical response to transverse deformation produced by a micro-displacement. In order to characterize the micro-displacement dependency, the sensor was firstly attached to a polished machined part. Facing it, a second polished machined part was placed. This second part presented a rectangular prominence 1.5 mm long and 5 mm deep. Once centered on the HCF section, this protrusion would be responsible for the transverse deformation on the sensor. In order to avoid fiber breakage when the machined parts approached, its edges were slightly smoothed, (see Fig. 1 (b)). Its particular dimensions were the smallest possible when considering the accuracy of the vertical milling machine employed. Consequently, the final design of the sensor presented a 3 mm long HCF section, so that the deformation was restricted to the hollow section of the sensor. In this way, deformation in the SMF that could interfere with the measurement was avoided. Moreover, splices were not subjected to an unnecessary stress that could cause them to break, thus limiting the measurement range. Finally, to avoid the effect of unintended reflections, the end of the SMF section of the sensor not connected to the interrogator was trimmed at 8º.

The machined parts rested on a motorized station that provided a resolution of 17 nm in their spacing, thus delimiting the measurement range to micro-displacements.

With the aid of an optical microscope, the machined parts were initially positioned so the 1.5 mm long protrusion was located approximately 40 µm away from the sensor. Once in place, the machined parts were approached at a rate of 85 nm per step until reaching the sensor surface. From this point, another 37.5 µm were advanced, now transversely deforming the HCF. At each step, the spectral response of the sensor was acquired in the 1510 to 1590 nm range by means of an optical sensor interrogator (OSI, Micron Optics sm130) with a spectral resolution of 2.4 pm. These spectra were then analyzed in the spatial frequency domain by applying the Fast Fourier Transform (FFT) algorithm, which is the domain over which the response of the sensor to transverse micro-displacement was studied.

4. Theoretical Analysis

As a first approximation, an SMF-HCF-SMF structure such as the one designed can be physically identified with a Fabry-Perot (FP) etalon, in which the propagation in the HCF section is performed by anti-resonance. Moreover, as a consequence of its low finesse ($F < 1$), its reflectance, R, can be expressed as [4]:

$$R \propto 1 - \cos\left(\frac{4\pi}{\lambda_0} nL\right), \qquad (1)$$

where n is the refractive index of the medium ($n = 1$), L is the length of the etalon ($L = 3$ mm), and λ_0 is the wavelength considered. From this expression, the distance, $\Delta\lambda_m$, between two consecutive wavelengths of maximum reflectance, λ_m and λ_{m+1}, is of the form $\Delta\lambda_m \approx \lambda_m^2/(2nL)$. This distance can be interpreted as a continuously variable period of reflectance, and its inverse as the associated spatial frequency, $f = 1/\Delta\lambda_m = 2nL/\lambda_m^2$.

Considering this relationship and the spectral range of the OSI employed, $\lambda_m(nm) \in [1510, 1590]$, significant spatial frequencies in the transformed domain were to remain in $f \in [2.37, 2.63]\ \mathrm{nm}^{-1}$. Moreover, the spatial frequency resolution of $1.25 \cdot 10^{-2}\ \mathrm{nm}^{-1}$ was also determined by the spectral range. Within this frequency range, however, the particular functional form was not easy to foresee, since the structure´s behavior was not completely determined by a single propagated mode, but rather exhibited a multimodal nature in the HCF region.

To determine the number of substantially excited modes in the HCF section, as well as their effective refractive indices, a suite of robust and fully vectorial mode solvers for waveguide structures was used (PhotonDesign Fimmwave & Fimmprop). The result was that 4 circular symmetry anti-resonant modes, corresponding to HE_{11} to HE_{14}, were enough to explain 94 % of the optical power propagated in the structure. These modes had effective

refractive indices ranging from 0.99975 to 0.99403 at 1550 nm. As can be seen, the difference in effective refractive indices between modes, and with respect to the air refractive index considered in the FP model itself, remained under $6 \cdot 10^{-3}$. This implied corrections in the spatial frequency domain lower than 10^{-2} nm^{-1}, which were just under the FFT resolution. Thus, the FP model and conclusions regarding the transformed domain remained applicable, taking into account that, in the range of observable frequencies, the final functional form would result from the contribution of the FPs associated with each mode and not a single mode.

Once the range of spatial frequencies characteristic of the designed sensor was located, it was necessary to determine whether these frequencies would vary significantly with transverse micro-displacements. The reasoning is that, once the displacement beyond contact began, the geometry of the structure would be altered. In this regard, it can be proven that the propagation constants for circular and elliptical fibers are identical for slight eccentricity, provided the core areas remain equal [5]. This was one of the main reasons for limiting the study to a maximum displacement of 37.5 µm, corresponding with a 30 % deformation. Thus, it was expected that the spatial frequency components would remain nearly constant, allowing the transversal micro-displacement to be monitored by the phase of some of them, which is much more sensitive to perturbations of any nature.

5. Results and Discussion

The spectra obtained for the different values of transverse micro-displacement are shown in Fig. 2 (a). As can be seen, all of them exhibited the presence of multiple beats associated with the multimodal nature of the sensor, with a remarkably fast carrier as a consequence of its large length. Furthermore, it can be observed in Fig. 2 (b) that, as the micro-displacement increased, both attenuation and shift of the spectrum took place, but without a significant disturbance of its functional form. This result, consistent with the previous theoretical analysis, is especially remarkable when studying the spatial frequency domain by means of FFT.

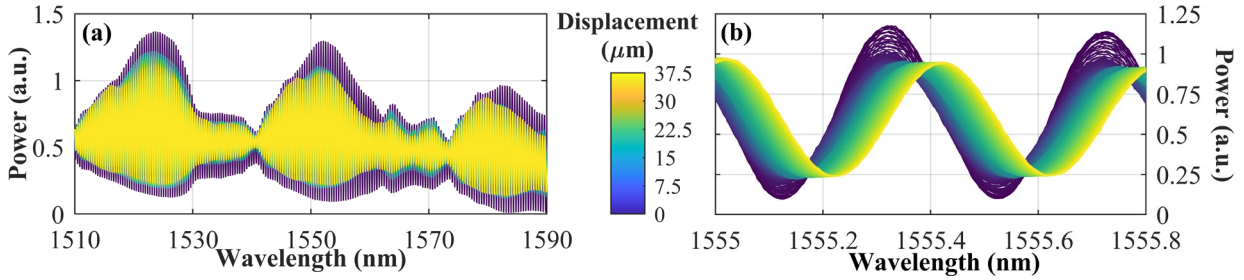

Fig 2. Sensor reflectance and its dependency with transverse micro-displacement (a), and a detailed view around the center of the spectrum (b).

As shown in Fig. 3 (a), spatial frequencies other than zero remained in the range associated with their behavior as an FP-etalon. The detail shown in Fig. 3 (b) illustrates that, even with their multimodal nature, there were mainly three distinct spatial frequencies with significant contribution. Moreover, their values remained constant over the entire range of displacements. Therefore, their phase could be reliably monitored.

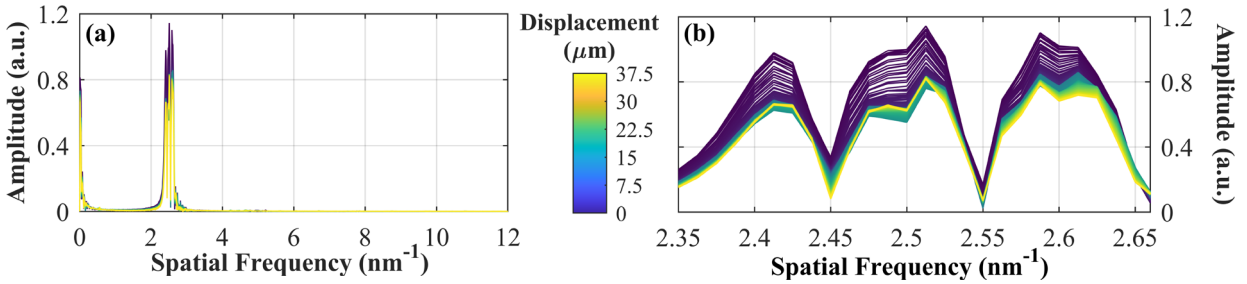

Fig 3. Amplitude of the FFT from the spectrum of Fig. 2 (a), and a detailed view around the range of interest (b).

The study of any of the three main observed frequencies yielded similar results, so we limit ourselves to present those associated with the narrowest spatial frequency, $f = 2.4125$ nm^{-1}. The monitoring of its phase for different values of micro-displacement is shown in Fig. 4 (a). Here, the measurements taken previously to reaching the sensor surface have also been included as negative displacements. As it can be observed, the phase remained constant until the last 8 µm. From this point on, the proximity of the machined part to the fiber influenced the optical propagation within the structure, causing the appearance of a brief transient. However, once the contact was made, the phase varied linearly with the micro-displacement, with a sensitivity of $-4.35 \cdot 10^{-2}$ rad/µm and a coefficient of determination of

0.9989. Fig. 4 (b) shows how the sensing threshold of the designed monitoring system was not reached, being able to optically resolve displacements of the order of tens of nanometers. Compared to previously developed micro-displacement sensors, the detection threshold has been improved by almost two orders of magnitude, at the cost of reducing the measurement range by an order of magnitude [6].

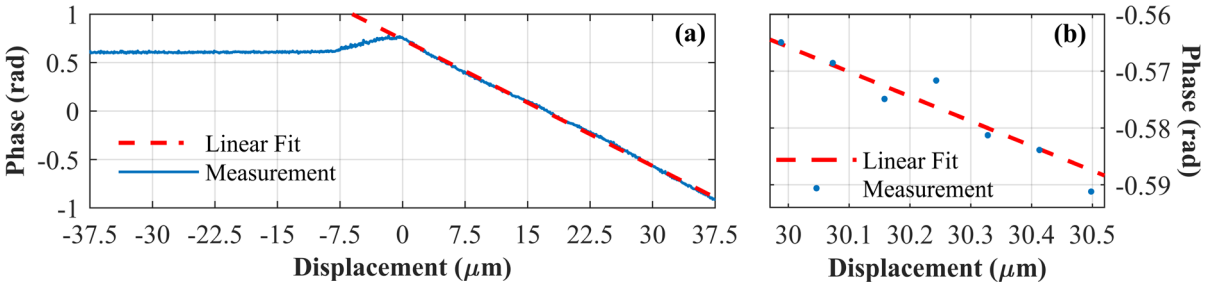

Fig 4. Phase variation of the selected spatial frequency as a result of transverse micro-displacement (a), and a detailed view (b).

Thus, for the first time to our knowledge, the feasibility of using HCF-based interferometers as micro-displacement sensors has been tested. Moreover, the response of the sensor has been found to be linear over the entire range considered. In fact, given that this range has been limited to 30 % of the original fiber diameter, the HCF section of the sensor can be modelled as an isotropic elastic continuous material [7]. As a fundamental property of this type of material, the transverse deformation caused has to be linear with the pressure exerted. Consequently, the phase of the spatial frequency itself must be linear with the exerted pressure, and thus the designed sensor is also suitable as a transversal pressure sensor. This result is particularly relevant, for example, in the detection of steel corrosion distributed in reinforced concrete structures [8]. The development of a setup for its experimental characterization is, however, still in progress.

6. Conclusions

This work has presented a Fabry-Perot etalon-type interferometric structure as a novel micro-displacement sensor. Its design was based on a 3 mm long hollow core fiber section fused to standard single-mode fibers at both ends. The manufacturing process was optimized to achieve sensor length accuracies of 1 micron, guaranteeing its reproducibility. The expected optical response in the spectral and transformed domains were theoretically analyzed, emphasizing in its multimodal interferometric nature. This analysis was verified experimentally, characterizing its behavior under transverse micro-displacements by monitoring the phase of one of the spatial frequencies associated with its reflectance. The obtained result was a linear response with a sensitivity of $-4.35 \cdot 10^{-2}$ rad/µm, a determination coefficient of 0.9989, and a sensing threshold under 85 nm. Finally, since the transverse deformation of the sensor in the micro-displacement range studied remained linear with the applied pressure, the feasibility of the proposed structure as a directional pressure sensor was also suggested.

7. Acknowledgements

This work is part of the projects PID2019-107270RB-C02, funded by MCIN/AEI/10.13039/501100011033 and FEDER “A way to make Europe”, and PDC2021-121172-C01 funded by MCIN/ AEI/10.13039/501100011033 and European Union “Next generationEU”/PTR.

8. References

[1] J. Harrington, "A Review of IR Transmitting Hollow Waveguides", Fibers and Integrated Optics **19**, 211-217 (2000).
[2] M. Hou et al., "Antiresonant reflecting guidance mechanism in hollow-core fiber for gas pressure sensing," Opt. Express **24**, 27890-27898 (2016).
[3] W. Sun et al., "Comparative Study on Transmission Mechanisms in a SMF-Capillary-SMF Structure," J. Lightwave Technol. **38**, 4075-4085 (2020).
[4] J. L. Santos, A. P. Leite, and D. A. Jackson, "Optical fiber sensing with a low-finesse Fabry–Perot cavity," Appl. Opt. **31**, 7361-7366 (1992).
[5] A. W. Snyder and J. D. Love, *Optical Waveguide Theory* (Chapman & Hall, 1983), Chap. 18.
[6] M. Bravo et al., "High precision micro-displacement fiber sensor through a suspended-core Sagnac interferometer," Opt. Lett. 37, 202-204 (2012).
[7] S. Timoshenko and J. N. Godier, *Theory of elasticity* (McGraw-Hill, 1951), Chap. 1.
[8] C. McCague et al., "Novel Sensor Design Using Photonic Crystal Fibres for Monitoring the Onset of Corrosion in Reinforced Concrete Structures," J. Lightwave Technol. **32**, 891-896 (2014).